Hindawi
Shock and Vibration
Volume 2023, Article ID 3188065, 12 pages
https://doi.org/10.1155/2023/3188065

Research Article

Estimating Site Characteristic Parameters of the Gobi Desert Region Using Seismic Noise

Ya Li,[1] Shengyang Chen ,[2] and Jie Lei[2]

[1]*Department of Civil Engineering, Shanghai Normal University, Shanghai 201418, China*
[2]*College of Civil Engineering, Tongji University, Shanghai 200092, China*

Correspondence should be addressed to Shengyang Chen; chenshengyang@tongji.edu.cn

Received 1 March 2023; Revised 28 June 2023; Accepted 3 July 2023; Published 13 July 2023

Academic Editor: Denise-Penelope Kontoni

In the Gobi desert region, the predominant frequency of the horizontal-to-vertical spectral ratio (HVSR) curve of seismic noise ($f_{H/V}$) is typically above 3 Hz. However, most of the existing formulas for estimating cover thickness (H) based on $f_{H/V}$ are only applicable for $f_{H/V}$ values below 5 Hz. Therefore, new formulas that can accurately calculate H in this region are crucially needed. To this end, a case study was conducted where noise measurements were carried out in the Gobi region in China, as well as in the east and northeast regions of China. The HVSR curves and $f_{H/V}$ were calculated, and a formula that correlates $f_{H/V}$ with H was derived. In addition, formulas that correlate with V_{s20} (average shear-wave velocities to depth 20 m) and V_{s30} (average shear-wave velocities to depth 30 m) $f_{H/V}$ were fitted. The relationship between the site fundamental period (T_s) and $T_{H/V}$ ($1/f_{H/V}$) was also investigated. Finally, by using all of the noise measurements and applying the derived relationships, a method for rapidly measuring the site type was proposed. The results showed that the equation for calculating H in this paper is highly reliable, with relative errors less than 30% compared to other researchers. The correlation between $f_{H/V}$ and V_{s30} was higher than that between $f_{H/V}$ and V_{s20}. The accuracy rate of the proposed method for fast identification of ground types was greater than 80%.

1. Introduction

It is widely accepted amongst the earthquake engineering community that ground geology has a significant effect on ground motion [1–4], and the seismic design codes determine the design response spectrum according to the ground types for seismic fortification. In recent years, two critical parameters for identifying ground types are H (thickness of sediment) and V_{sz} (average shear-wave velocities to depth z) [5–7]. For example, the Chinese code for seismic design of building uses H and V_{s20} (average shear-wave velocities to depth 20 m) to piecewise site types [8], while Eurocode 8 [9] employs V_{s30} (average shear-wave velocities to depth 30 m) as the only parameter for ground type identification. Hence, estimating H, V_{s20}, and V_{s30} is a matter of great importance in civil engineering.

Boreholes, excavations, and other geotechnical investigations are primary methods for measuring H and V_{sz} [4]. However, these methods are often prohibitively expensive. Though leveraging geophysics may reduce costs, most techniques are challenging to deploy in urban areas. To overcome those limitations, several researchers have employed the microtremor horizontal-to-vertical spectral ratio (HVSR) technique to measure H and V_{sz} (e.g., [4, 10–17]).

The microtremor HVSR technique, also known as the Nakamura technique [18, 19], is widely used to analyze the ground dynamic characteristics due to its high cost-effectiveness in the survey and negligible interference with the environment [20, 21]. The microtremor HVSR has been utilized in various studies, such as in the Grenoble basin [22], Thessaloniki basin [23], and Trabzon-Arsin basin [24], to investigate the seismic response of sites in the frequency domain and evaluate the resonance frequency of sediments.

Due to the close relationship between the resonance frequency of the sediments and the subsurface structure and geotechnical parameters (e.g., H and V_{sz}), Ibs-von Seht and Wohlenberg [12] used the microtremor HVSR to calculate H

for the first time and found that the main peak frequency of the microtremor HVSR curve ($f_{H/V}$) correlates well with H and then established a quantitative relationship between H and $f_{H/V}$ for Lower Rhine Embayment (Germany). Since then, Delgado et al. [25] and Parolai et al. [4] fitted new relationships to calculate H and V_{sz} for the region in Spain and Cologne Area, respectively. However, in those studies, the relationships between H and $f_{H/V}$ are valid for soils from a few tens of meters to more than 1000 m thick. Also, Lin and Wang [26] investigated that the $f_{H/V}$ for Gobi desert in China ranged from 3 Hz to 14.2 Hz. Moreover, more than 90% of the sediment thickness in boreholes in the Gobi desert is less than 20 m, with half being less than 5 m. Therefore, the relationships between $f_{H/V} - H$ and $f_{H/V} - V_{sz}$ that have been fitted previously are inadequate for Gobi desert in China.

H, V_{s20}, and V_{s30} have been widely used as site class delineators; nonetheless, many studies have shown that those parameters are not adequate to distinguish the ground classification [7, 27]. Thus, efforts have been made in the search for alternative site proxies to H, V_{s20}, and V_{s30}. Zhao et al. [28] proposed using T_0 (fundamental period of site) and horizontal-to-vertical (H/V) response spectral ratios over a wide period range to classify K-NET stations in Japan and developed a GMM using the period-based classification scheme. Hassani and Atkinson [29] have concluded that T_0 was superior to V_{s30} in identifying site effects in central and eastern North America. Meanwhile, in California, Hassani and Atkinson [30] was able to achieve an additional 5% reduction in the standard deviation of residuals by incorporating T_0 into the model after accounting for site effects related to V_{s30} and $Z_{1.0}$ (depth to $V_S = 1.0$ km/s).

Based on the abovementioned literature review, the following points are the main conclusions:

(a) The microtremor HVSR method is widely applied in calculating H and V_{se} in urban areas due to its cost-effectiveness and noninvasive nature to the environment.

(b) The existing microtremor HVSR method for calculating H and V_{se} is suitable for sites with the predominant frequency of HVSR below 5 Hz. However, it is not applicable to Gobi desert and similar areas, where the predominant frequency of HVSR ranges from 3 Hz to 14 Hz.

(c) H and V_{se} are the most widely used site class delineators; nonetheless, those parameters are not adequate to distinguish the site effects at one site from those at another site period.

In order to derive a new formula for accurately calculating H and V_{se} for the Gobi desert and expand the applicable range of the formula variables, as well as to enable fast identification of ground types based on microtremor HVSR, noise measurements were carried out in China. Then, the HVSR curves were calculated and analyzed. On this basis, a study was conducted to investigate the relationship between site characteristic parameters (H, V_{s20}, V_{s30}, and T_s) and the dominant frequency of the HVSR curve. By using all of the noise measurements and applying the derived relationships, a method for fast identification of ground types based on the microtremor HVSR was proposed. Moreover, the discussion section compares the research findings of this study with the research results of other scholars.

2. Methodology

A total of 85 boreholes are collected and plotted in Figure 1(a), which are divided into three groups based on location: west sites (including 45 boreholes, located in Gobi desert), northeast sites (including 36 boreholes), and east sites (including 4 boreholes). The corresponding H and V_{s30} (calculated using equation (1)) for all 85 boreholes are illustrated in Figures 1(b) and 1(c), respectively. As shown in the figures, the minimum and maximum H values for the west sites were 5 m and 100 m, respectively. Furthermore, 76% of these sites had a cover thickness of less than 20 m, with only one site exceeding 90 m. The V_{s30} values for the west sites are evenly distributed between 300 m/s and 700 m/s. Conversely, the east sites exhibited H values greater than 100 m and V_{s30} values less than 200 m/s. As for the northeast sites, the H values ranged from 20 m to 100 m and the V_{s30} values ranged from 100 m/s to 250 m/s. Overall, the H values for the west sites are smaller than those of the northeast and east sites, while the V_{s30} values are greater, indicating that the west sites are harder than the other two locations. The western sites are located around the Junggar basin, which is characterized by a substantial amount of sedimentary deposits. These deposits primarily include sandstone, conglomerate, mudstone, and coal seams. The northeast sites and west sites are located in plain areas, primarily composed of clay and silty clay, respectively. The soil in these sites is composed of three layers in general, with 0–7 m of the top layer filled.

Seismic noise measurements are conducted in close proximity to the drilling sites using the TAG-33M accelerometer (Figure 2). The TAG-33M accelerometer, which integrates a sensor and a data collector, is used for measuring microtremors in three directions. This accelerometer is ideal for field measurements and other applications. It features an antioxidation aluminum casing, waterproof connectors, and stainless steel leveling and fixing screws, which allow it to function under challenging field conditions. The compact device is simple to install and troubleshoot. In addition, the accelerometer has a sampling frequency range of 0.001 Hz–200 Hz and is capable of operating at temperatures ranging from −40°C to 60°C, making it suitable for the low-temperature conditions of the winter sites.

The installation procedure for recording ground seismic noise using the TAG-33M accelerometer is as follows [31]:

(a) After selecting the appropriate installation location, we use a compass to mark the true north and east directions on the surface and then drill a D8 mm × 45 mm hole at the installation location using an impact drill (Figure 3(a))

(b) We insert an M6 × 60 expansion screw into the hole (Figure 3(b))

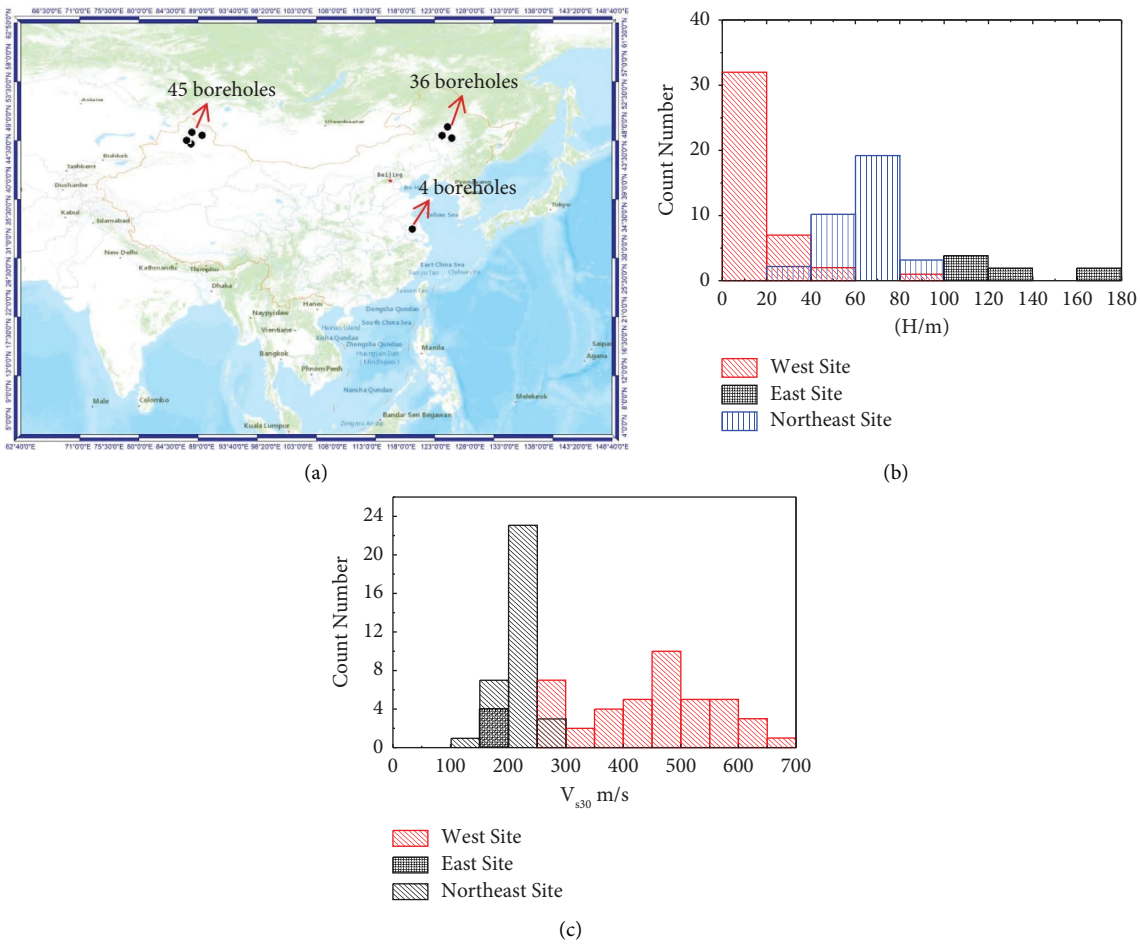

Figure 1: Distribution of the collected boreholes (a) and the statistic of site parameters (b, c). (a) The location of 85 boreholes (the solid circle represents the borehole location), (b) the statistic of H, and (c) the statistic of V_{s30}.

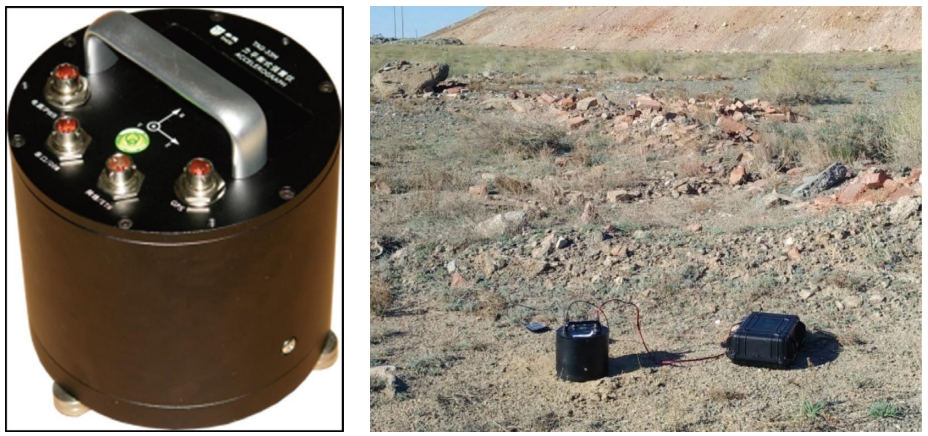

Figure 2: Seismic noise measurement. (a) TAG-33M accelerometer and (b) measuring noise in the Gobi desert.

(c) We loosen the nut and place the accelerometer in the center position and then tighten the nut to secure it onto the accelerometer's clip

(d) We adjust the orientation of the accelerometer and then adjust the leveling screws until the bubble is centered (Figure 3(c))

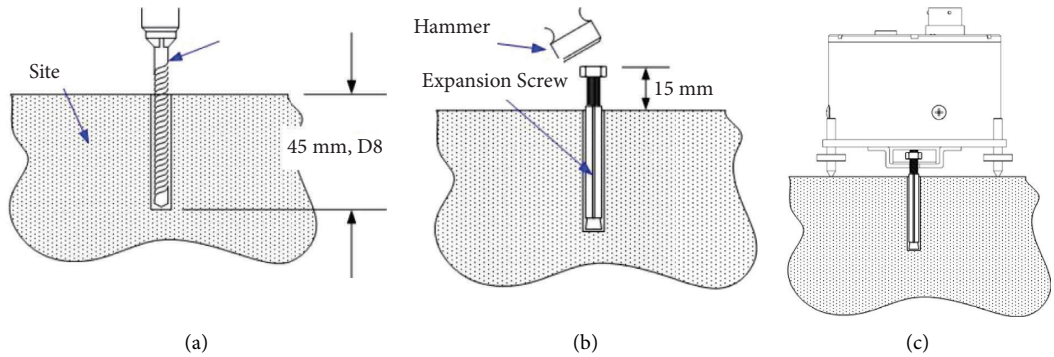

Figure 3: The installation procedure for TAG-33M: (a) drill a D8 mm × 45 mm hole, (b) insert expansion screw, and (c) installation illustration.

To ensure reliable microtremor recordings, two instruments were placed on the same borehole. Each recording lasted 25 minutes, with a sampling rate of 100 Hz. The resulting signals from all three directions (up-down, north-south, and east-west) are displayed in Figure 4.

$$V_{S30} = \frac{30}{\sum_{i=1}^{n} d_i / v_i}, \quad (1)$$

$$V_{S20} = \frac{d_0}{\sum_{i=1}^{n} d_i / v_i}. \quad (2)$$

d0 is the smaller value between the thickness of the cover layer and 20 m, di is the thickness of the ith layer, and v_i is the shear wave velocity of the ith layer.

3. Calculation and Analysis of the HVSR Curve

A Hanning window with a 28% bandwidth was chosen because it provided sufficiently good smoothing without suppressing significant features in the spectrum. Following the Site Effects Assessment using AMbient Excitations (SESAME) criteria [32], the signal relative to each window was detrended, baseline corrected, tapered, and band-pass filtered between 0.1 and 25 Hz. The fast Fourier transform of the three signal components for each analysis window was then performed, and the HVSR curves were determined using equation (3). The main peak frequency of the HVSR curve for the 85 sites is listed in Table 1. It is worth noting that although the sampling frequency was 100 samples, the spectral range shown was limited to 0.1–20 Hz, which is typically considered appropriate for studies of seismic microzoning and earthquake engineering.

$$\frac{H}{V} = \frac{\sum_{i=1}^{n} \sqrt{H_{EW(i)}^2 + H_{NS(i)}^2 / 2V^2}}{n}, \quad (3)$$

As presented in Table 1, the main peak frequency of the HVSR curve exhibited a range of 0.58 Hz–12.5 Hz across the 85 sites investigated. For the west sites, described in Figure 1(a) and labeled 1 to 45, the predominant frequency range of the HVSR curve was between 1.1 Hz and 12.5 Hz. As for the northeast sites (labeled 46 to 81), the predominant frequency range of the HVSR curve was between 1.0 Hz and 4.9 Hz, while for the eastern sites (labeled 82 to 85), it was between 0.5 Hz and 1 Hz. Furthermore, based on the Chinese seismic code, the 85 sites were categorized into three groups (II, III, and IV) and their corresponding HVSR curves are presented in Figure 5.in which $H_{EW(i)}$ and $H_{NS(i)}$ indicate the NS and EW direction spectrum curves relative to the ith window, $V(i)$ indicates the up-down direction spectrum curves relative to the ith window, and n indicates the window number.

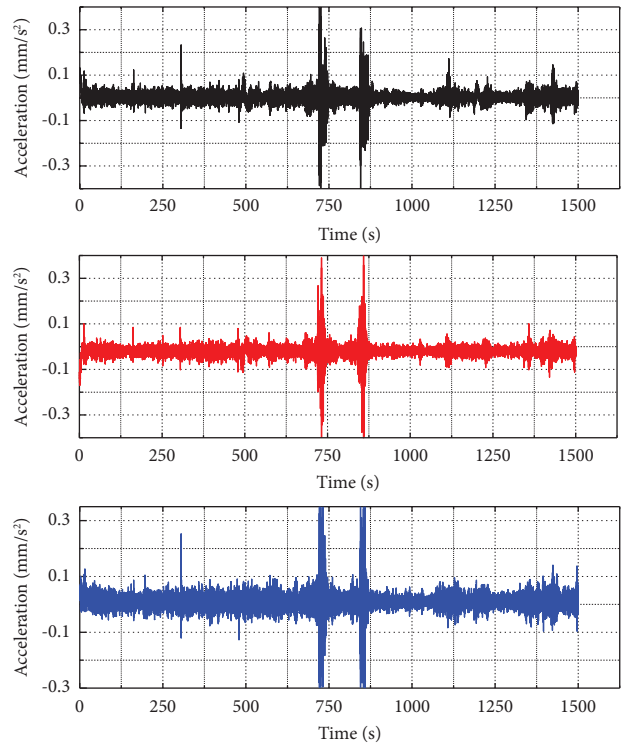

Figure 4: The resulting signals from all three directions for one site (the recordings are depicted in black, red, and blue, representing the north-south (NS), east-west (EW), and up-down (UD) directions, respectively).

As depicted in Figure 5, the shape of the HVSR curve varies considerably based on the ground type. For class IV sites, the HVSR curves exhibit a single peak and the predominant frequency is less than 1 Hz. In contrast, for

Table 1: The site parameters and predominant frequency of the HVSR curve for 85 sites.

Nos.	H (m)	V_{s20} m s^{-1}	V_{s30} m s^{-1}	$f_{H/V}$
1	6	318	555	7.8
2	13	353	482	7.6
3	9	406	626	12.5
4	5.2	394	583	10
5	13.5	430	524	7.2
6	12	418	559	8.9
7	6	391	679	12.5
8	15.5	339	423	10.2
9	16	382	461	6.8
10	14.2	377	471	8.1
11	5	250	550	12.7
12	14	404	504	6.6
13	13	323	468	5.9
14	20	349	417	6.6
15	11	317	510	13
16	18	387	454	5.9
17	21	333	384	5.5
18	5.8	362	584	11
19	8	417	615	12.5
20	6	314	617	12
21	8.7	267	462	5.6
22	10	298	453	9.2
23	17	340	410	4.8
24	19	274	338	3.6
25	18	274	356	4.5
26	16	268	370	4.4
27	10	274	422	8.9
28	9	280	430	9
29	8.7	290	450	10
30	39	262	279	3.2
31	34	257	269	3.3
32	20	261	277	5
33	28	267	300	5.5
34	27	234	278	5
35	40	254	270	2.0
36	42	224	251	2.0
37	18	327	369	6.7
38	12	324	480	7.0
39	14	344	408	3.6
40	5	450	650	12.1
41	42	230	225	1.6
42	13.5	270	590	10
43	8.7	267	458	10
44	8	319	498	8.3
45	10	303	502	8
46	16	265	280	5.1
47	96	230	257	1.0
48	42	215	241	2.0
49	70	188	213	1.4
50	78	180	197	1.4
51	68	180	205	1.8
52	84.5	184	204	1.3
53	68	188	209	1.4
54	75	225	244	1.3
55	90	181	212	1.3
56	58	177	199	1.3
57	58	152	175	1.7
58	78	182	201	1.2
59	55	164	190	1.8
60	52	215	249	1.9
61	76	164	184	1.5
62	72	177	198	1.1
63	54	165	194	1.9
64	76	191	216	1.3
65	81	219	243	1.1
66	76	207	236	1.3
67	70	207	238	1.3
68	64	193	217	1.1
69	61	189	224	1.1
70	72	196	221	1.1
71	64	229	255	1.0
72	64	205	223	1.3
73	64.5	226	249	1.2
74	65	224	241	1.3
75	46.6	172	206	1.3
76	46.5	182	210	1.6
77	51	181	213	1.4
78	43.8	193	225	1.6
79	75	225	249	1.3
80	21.5	241	295	4.9
81	23	244	289	3.49
82	176	150	160	0.58
83	100	171	171	1
84	130	161	182	0.8
85	102.3	152	166	0.9

harder sites such as class II and III, the HVSR curves have multiple peaks and the predominant frequency is greater than 1 Hz. Furthermore, the peak of the HVSR curve is more pronounced at higher frequencies for class II sites.

4. Uncertainties in Microtremor Data Analysis

The random nature of ambient noise (both in time and space) is a critical issue in microtremor data analysis [33, 34], particularly in densely populated areas such as the northeast and east sites due to industrialization and heavy traffic activities. To minimize such random ambient noise, microtremor data are preferably collected during early morning hours to achieve results closer to reality and ensure stability. However, in the Karamay area, since the measurement points are all located in uninhabited areas, the measurements are not limited to the morning. All measurement points are simultaneously measured using two instruments.

After the aforementioned steps, the HVSR curve is calculated and the peak is evaluated according to the SESAME project criteria. For HVSR curves with unclear peaks, we analyze them using methods described in Sections 3.2.1 and 3.2.2 of SESAME, as well as a clustering analysis method developed by our research group. The schematic diagram of the clustering analysis method is shown in Figure 6, and the specific steps are as follows:

(a) Microtremor HVSR curves are inputted, and K-means is used to cluster them into two main clusters 20 times

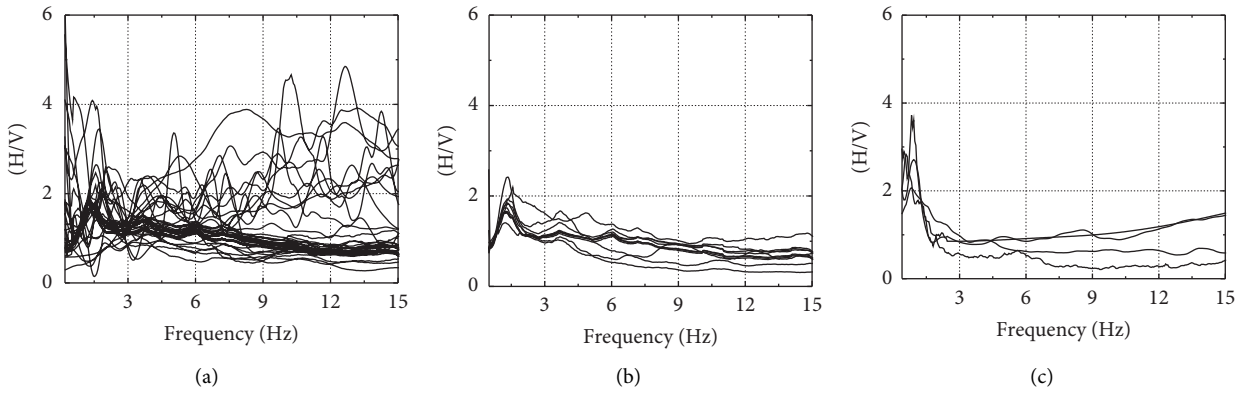

Figure 5: HVSR curves for different types of sites. (a) II, (b) III, and (c) IV.

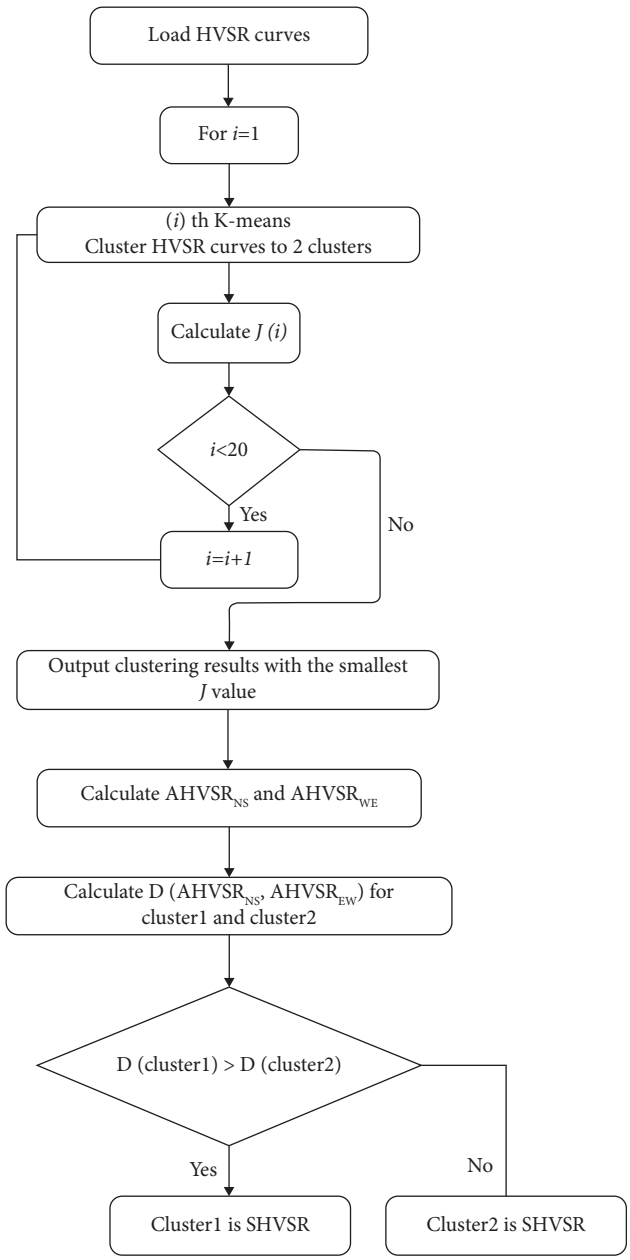

Figure 6: The detailed process for HVSR.

(b) For each cluster, the cost function (J) is calculated and the clustering output with the smallest J value is selected as the final result

(c) $AHVSR_{NS}$ (average HVSR for NS direction) and $AHVSR_{EW}$ (average HVSR for EW direction) curves for both clusters are then calculated

(d) The correlation distance between $AHVSR_{NS}$ and $AHVSR_{EW}$ for each cluster is calculated and compared

(e) The cluster HVSR curves with the smaller correlation distance are considered the SHVSR (HVSR for the site) curves

5. Site Characteristic Parameters

5.1. H − $f_{H/V}$ Relationship. Ibs-von Seht and Wohlenberg [12] demonstrated that the resonance frequency of the soil layer (f_r, which can be estimated from the peak in the HVSR curve) was closely linked to H using the following relationship:

$$H = a f_r^b. \tag{4}$$

Using the $f_{H/V}$ (listed in Table 1) and H obtained from the borehole data, a nonlinear regression fit of equation (4) was performed and obtained for the investigated area using the following equation:

$$H = 91.95 f_{H/V}^{-1.066}. \tag{5}$$

Values and standard errors of the correlation coefficients a and b are given in Table 2. Figure 7 shows the relationship between $f_{H/V}$ and H, where the distribution range of $f_{H/V}$ is 0.58 Hz~12.5 Hz, and the adjusted R-square value is 0.94 which is significantly greater than critical values of correlation coefficient $r(85-2)_{0.001} = 0.36259$. These results indicate a strong correlation between $f_{H/V}$ and H in the frequency range of 0.58 Hz–12.5 Hz.

5.2. $V_{s20} - f_{H/V}$ and $V_{s30} - f_{H/V}$ Relationships. V_{s20} (calculated using equation (2)) and V_{s30} (calculated using equation (1)) are two important parameters to classify the site; therefore, a fast method to estimate those parameters is

Table 2: The fitting formula coefficients.

	a	Standard errors	b	Standard errors	Adjusted R^2
H	91.95	1.67	−1.07	0.04	0.94
V_{s20}	183.07	6.84	0.28	0.02	0.70
V_{s30}	184.77	7.35	0.45	0.02	0.87
T_s	1.17	0.033	0.91	0.05	0.91

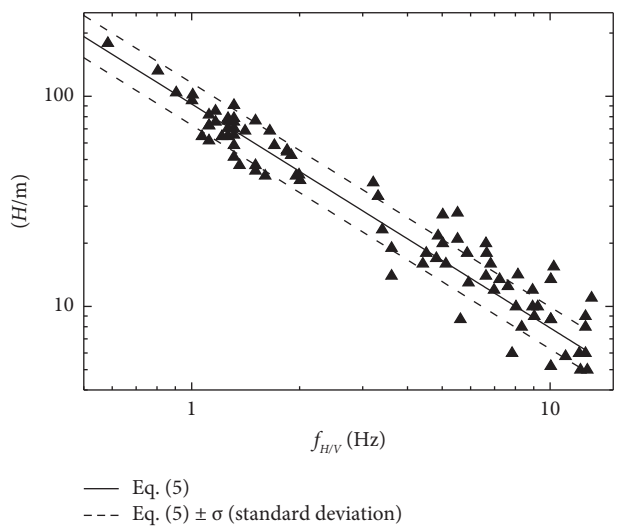

Figure 7: $f_{H/V}$ *vs.* H.

a matter of great importance. Delgado et al. [25] showed that the average shear wave velocity of the soft sedimentary column, V_s, can be related to H through a relationship of the following form:

$$V_S = cH^d, \tag{6}$$

$$V_S = c\left(af_{H/V}{}^b\right)^d = ef_{H/V}{}^g. \tag{7}$$

The relationship between H and $f_{H/V}$ was fitted by equation (4). By substituting equation (4) into equations (6) and (7), another equation was obtained. Thus, a nonlinear regression fit of equation (7) was performed using $f_{H/V}$, V_{s20}, and V_{s30}, resulting in the following equation for the investigated area:

$$V_{s20} = 119f_{H/V}{}^{0.52}, \tag{8}$$

$$V_{s30} = 147f_{H/V}{}^{0.57}. \tag{9}$$

Values and standard errors of the correlation coefficients a and b for the two equations are also listed in Table 2. Figure 8 shows the $f_{H/V}$*vs.* V_{s20} and $f_{H/V}$*vs.* V_{s30}. The adjusted R^2 values are 0.70 and 0.87, respectively, both of which are greater than $r(85{-}2)_{0.001} = 0.36259$. This suggests a strong correlation between $f_{H/V}$ and V_{s20} or V_{s30} in the frequency range of 0.58 Hz–12.5 Hz. Moreover, the higher R^2 value for the regression with V_{s30} indicates a stronger correlation between $f_{H/V}$ and V_{s30} than between $f_{H/V}$ and V_{s20}. In addition, while there is a strong correlation among V_{s20}, V_{s30}, and $f_{H/V}$ within the range of 0.58 Hz–12.5 Hz, the correlation among V_{s20}, V_{s30}, and $f_{H/V}$ is not significant within the range of 0.58 Hz–12.5 Hz.

5.3. $T_s - T_{H/V}$ Relationship. Several kinds of research studies have shown that the Nakamura method was fully established as an assessment method for the site fundamental period (T_s, calculate using equation (10), in which V_{sb} is the equivalent shear wave velocity, calculated using equation (11)); for accuracy-eliminated T_s using the HVSR method, the relationship between T_s and$T_{H/V}$ was studied.

$$T_s = \frac{4H}{V_{sb}}, \tag{10}$$

$$V_{sb} = \frac{H}{\sum_{i=1}^{n} d_i/v_i}, \tag{11}$$

in which H is the depth of the bedrock, d_i is the thickness of the ith layer, and v_i is the shear wave velocity of the ith layer.

Using the $T_{H/V}$ $(1/f_{H/V})$ and T_s, a nonlinear regression fit of equation (4) was performed and obtained for the investigated areas using the following equation:

$$T_s = 1.17T_{H/V}^{0.91}. \tag{12}$$

Figure 9 shows the regression curve of the $T_{H/V}$ and T_s, and the adjusted R^2 value is 0.91 which is greater than $r(85{-}2)_{0.001} = 0.36259$. It indicated that there is a strong correlation between $T_{H/V}$ and T_s in the range of 0.08 s–1.72 s. Besides, it can be seen from Figure 6 that when $T_{H/V}$ is less than 0.13 s, the points are evenly distributed near the red ($x = y$) line. However, when $T_{H/V}$ is greater than 0.13 s, the points are not distributed near the red line and trend towards the T_s-axis.

6. Identification of Ground Types

In China, the classification of ground types is based on Table 3 which uses two parameters, H and V_{s20}, to determine the site type. For example, a site is classified as type II when H and V_{s20} range from 3 m to 50 m and 150 m/s to 250 m/s, respectively. Using Table 3 and equations (5) (the red line in the figure) and (8) (the black line in the figure), Figure 10 is plotted. The boundaries of H (calculated using equation (5)) described in Table 3 are represented by L1, L3, and L5, while the boundaries of V_{s20} (calculated using equation (8)) are represented by L2, L4, and L6.

It can be seen from Figure 10 that when $f_{H/V} < 1.13$, H (calculate using equation (5)) is greater than 80 m; meanwhile, V_s (calculate using equation (8)) is less than 126 m/s; therefore, the ground type is IV (identify using Table 3). By the same token, the corresponding $f_{H/V}$ for the I, II, and III-

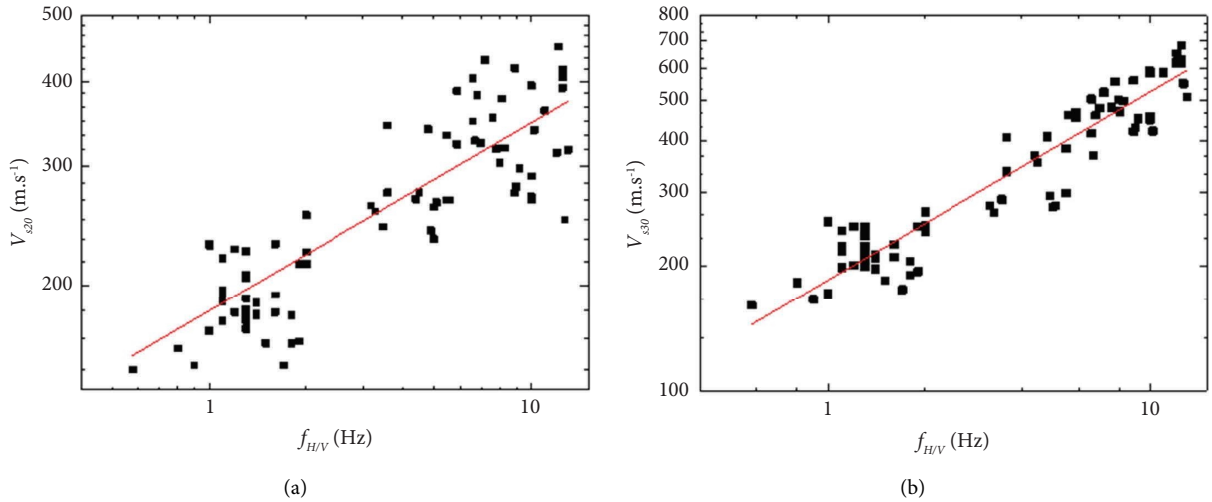

Figure 8: $f_{H/V}$ vs. V_{s20} and $f_{H/V}$ vs. V_{s30}. (a) $f_{H/V}$ vs. V_{s20} and (b) $f_{H/V}$ vs. V_{s30}.

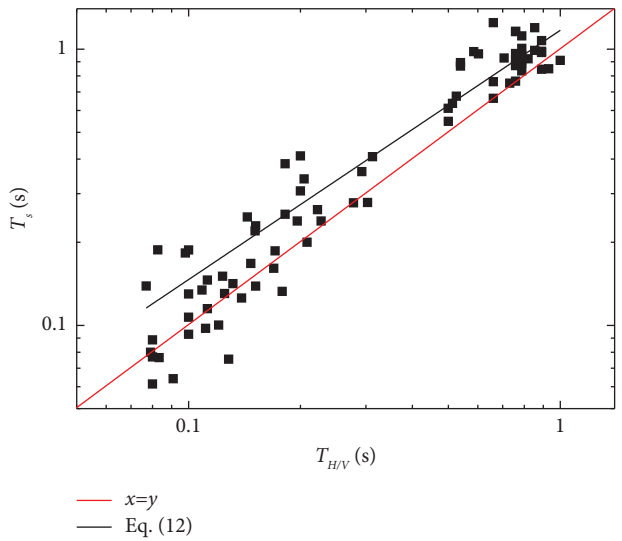

Figure 9: The regression curve of $T_{H/V}$ and T_s.

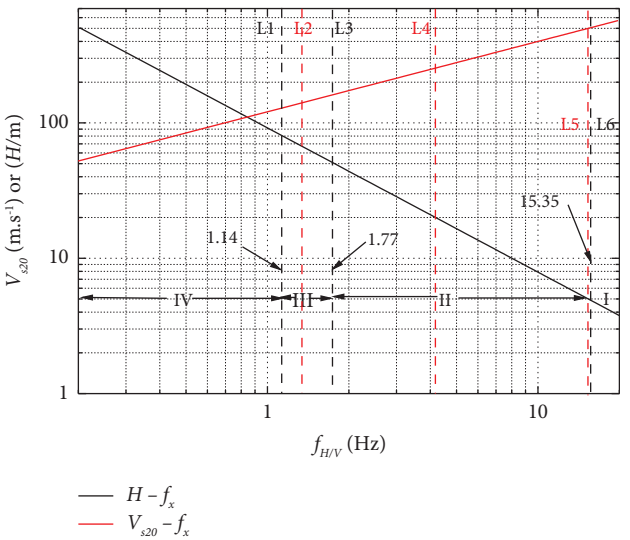

Figure 10: Identification of ground types (the red line represents the fitting curve of V_{s20} with $f_{H/V}$, while the black line represents the fitting curve of H with $f_{H/V}$. The dashed line indicates the intervals for site classification).

Table 3: Identification of ground types in China.

V_{S20} (m/s)	Ground types				
	I_0	I	II	III	IV
$Vs_{20} > 800$	0				
$800 \geq V_{S20} > 500$		0			
$500 \geq V_{S20} > 250$		< 5 m	≥5 m		
$250 \geq V_{S20} > 150$		< 3 m	3 m~50 m	>50 m	
$V_{S20} \leq 150$		< 3 m	3 m~15 m	15 m~80 m	>80

Note. This table is from Chinese code: code for seismic design of buildings. The numerical intervals in the table represent the cover thickness.

type sites is in the range >15.35 Hz, 1.77 Hz–15.35 Hz, and 1.13 Hz–1.77 Hz, respectively. The method for fast identification of ground types based on microtremor HVSR is listed in equation (13).

$$\begin{cases} I & f/_{H/V} \geq 15.35, \\ II & 15.35 > f_{H/V} \geq 1.77, \\ III & 1.77 > f_{H/V} \geq 1.13, \\ IV & f_{H/V} < 1.13. \end{cases} \quad (13)$$

7. Discussion

Table 4 presents two different relationships between H and $f_{H/V}$ derived by Ibs-Von and Craig, respectively. Figure 11 shows a comparison between equation (5) and those relationships. It should be noted that equation (5) was derived from data for $0.58 < f_{H/V} < 12.5$, while the equations derived

Table 4: $f_{H/V}$ – H for different researchers.

Researchers	a	Standard errors	b	Standard errors	Adjusted R^2
This paper	91.95	4.07	−1.066	0.145	0.596
Ibs-von	96	4	−1.388	0.025	0.98
Craig	70.253	4.946	−0.863	0.059	0.98

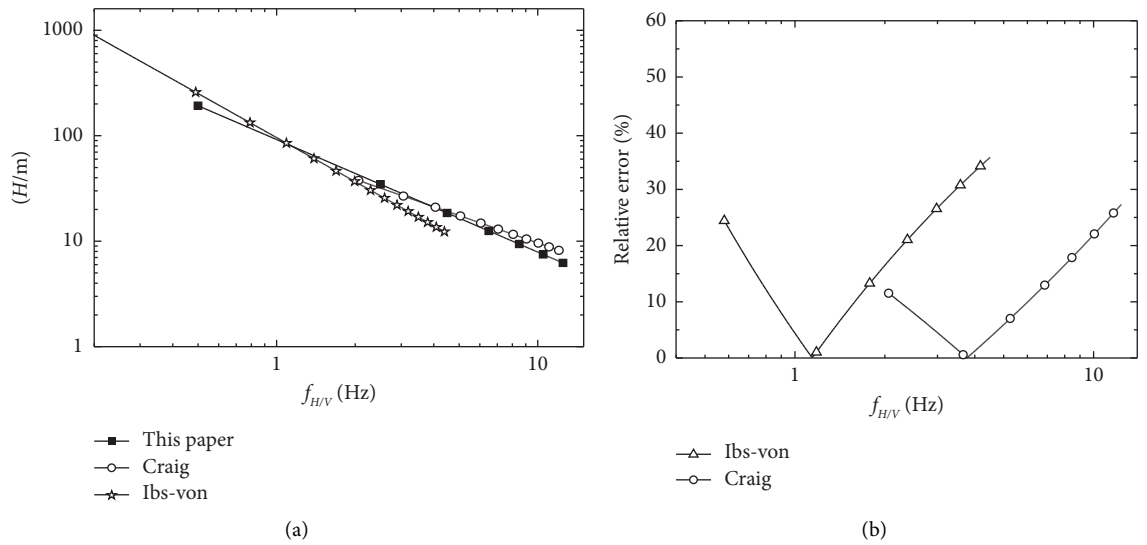

Figure 11: The comparison of equation (3) with other researchers. (a) The curve comparison and (b) the relative error.

by Ibs-Von and Craig were based on data for $0.14 < f_{H/V} < 4.5$ and $2.06 < f_{H/V} < 12.39$.

In the frequency range of 0.14–4.5 Hz, the relative error between equation (5) and Ibs-Von's equation is below 40% and the relative error is below 20% in the frequency range of 0.58–2.5 Hz. However, at higher frequencies (1–4.5 Hz), equation (5) gives deeper depths of the bedrock than those calculated by Ibs-Von's equation and the relative error increases as the frequency increases. In the frequency range of 2.06–12.39 Hz, the relative error is below 30% between equation (5) and Craig's equation. Figure 12 provides a detailed comparison between equation (5) and Ibs-Von's equation. It can be observed that, for Ibs-Von's equation, there is only one site that $f_{H/V} > 2.5\,Hz$, which could lead to inaccurate calculation of the formula at higher frequencies. All these comparisons indicated that equation (5) is valid for the calculated H.

A total of 178 boreholes were gathered from the literature sources Qi [35] and Chen [36], which included the borehole database and $f_{H/V}$ data. These boreholes were classified based on Table 3 into 102 II-type sites, 70 III-type sites, and 6 IV-type sites. The statistics of H and V_{s20} for these boreholes are shown in Figures 13(a) and 13(b). The H values of the 178 boreholes are evenly distributed from 5 m to 120 m, with a minimum of 7.5 m and a maximum of less than 120 m. The V_{s20} values range from 100 m/s to 400 m/s.

Two methods were used to classify the 178 sites based on their ground types: the method described in Section 6 and the TSSM [37]. The results are shown in Figure 14, where the black and red lines represent the demarcation lines based on

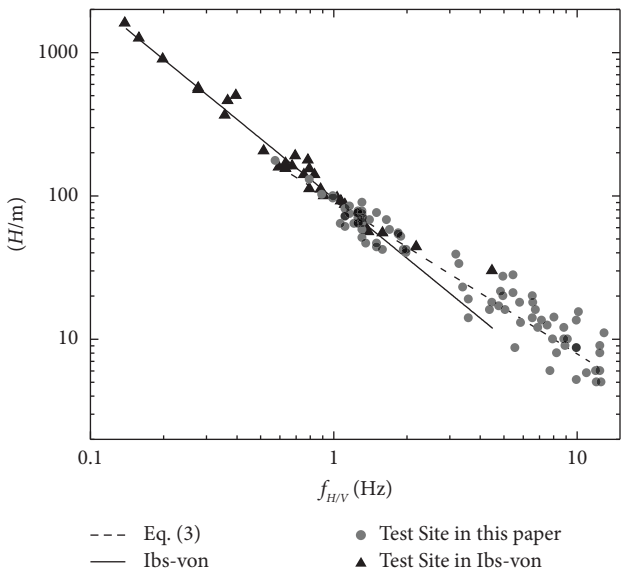

Figure 12: The detailed comparison of equation (5) with Ibs-Von's equation.

the two methods, respectively. The accuracy rate (R, calculated using equation (14)) for equation (13) in identifying the site types (II, III, and IV) was 81%, 98%, and 83%, respectively, all of which were above 80%. In contrast, the accuracy rate (R) of the TSSM method in identifying site types was 100%, 0%, and 47%, respectively, unable to accurately identify III-type sites.

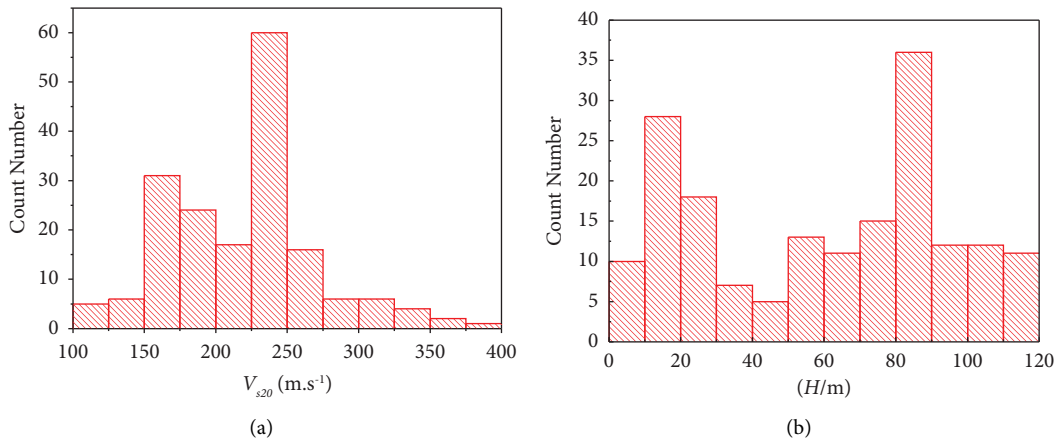

Figure 13: The statistic of V_{s20} and H for 178 boreholes. (a) The statistic of V_{s20} and (b) the statistic of H.

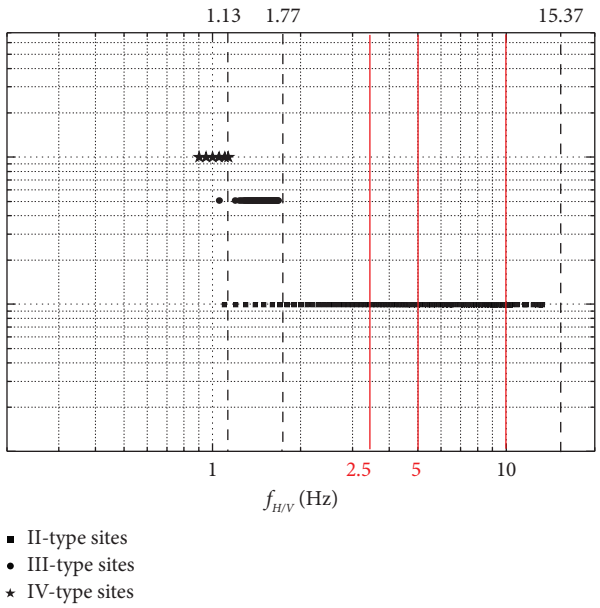

Figure 14: The classification results and the comparison of this paper method and TSSM (the solid red line is derived from TSSM, while the dashed black line represents the findings of this study).

$$R = \left(\frac{N}{T}\right) \times \%, \tag{14}$$

in which N is the right site number and T is the total site number.

8. Conclusions

This work aims to investigate the relationships of $f_{H/V} - H$, $f_{H/V} - V_{sz}$, and $T_s - T_{H/V}$ for the Gobi region and expand the applicable range of the relationships variables. Applying the derived relationships, a method to quickly determine the site type was proposed. The following points are the main conclusions drawn from this work:

(a) The shape of HVSR varies significantly depending on the ground type. For class IV sites, the HVSR curves exhibit a single peak, with the predominant frequency being less than 1 Hz. However, for harder sites such as class II and III sites, the HVSR curves show multiple peaks and the predominant frequency is greater than 1 Hz.

(b) In the frequency range of 0.58 Hz–12.5 Hz, there is a strong correlation between $f_{H/V}$ and H. The equation to calculate H in this paper exhibited high reliability with relative errors less than 30% compared to other researchers.

(c) In the frequency range of 0.58 Hz–12.5 Hz, there is a strong correlation between $f_{H/V}$ and V_{s20} as well as V_{s30}, with a stronger correlation observed between $f_{H/V}$ and V_{s30} than between $f_{H/V}$ and V_{s20}.

(d) There is a strong correlation between $T_{H/V}$ and T_s within the range of 0.08 s–1.72 s.

(e) The method for fast identification of ground types based on microtremor HVSR achieved an accuracy rate exceeding 80% for 178 sites. Specifically, the accuracy rates for the three types of sites (II, III, and IV) were 81%, 98%, and 83%, respectively.

Symbols

$f_{H/V}$: Predominant frequency of the HVSR curve
H: Cover thickness
V_{s20}: Average shear-wave velocities to depth 20 m
V_{s30}: Average shear-wave velocities to depth 30 m
T_s: Fundamental period of the site
$T_{H/V}$: Fundamental period of the HVSR curve
V_{sz}: Average shear-wave velocities to depth z
f_r: Predominant frequency of site
V_s: Average shear wave velocity of the soft sedimentary
d_i: The thickness of the ith layer
v_i: The shear wave velocity of the ith layer.

Data Availability

The data that support the findings of this study are available from the corresponding author upon reasonable request.

Conflicts of Interest

The authors declare that they have no conflicts of interest.

Acknowledgments

This work was supported by the Theoretical Study on Flexural Behavior of Precast Concrete Sandwich Panel (grant no. 52208181).

References

[1] İ. Akkaya and A. Özvan, "Site characterization in the Van settlement (Eastern Turkey) using surface waves and HVSR microtremor methods," *Journal of Applied Geophysics*, vol. 160, pp. 157–170, 2019.

[2] L. A. Atik, N. Abrahamson, J. J. Bommer, F. Scherbaum, F. Cotton, and N. Kuehn, "The variability of ground-motion prediction models and its components," *Seismological Research Letters*, vol. 81, no. 5, pp. 794–801, 2010.

[3] D. M. Boore, J. P. Stewart, E. Seyhan, and G. M. Atkinson, "NGA-West2 equations for predicting PGA, PGV, and 5% damped PSA for shallow crustal earthquakes," *Earthquake Spectra*, vol. 30, no. 3, pp. 1057–1085, 2014.

[4] S. Parolai, P. Bormann, and C. Milkereit, "New relationships between *vs*, thickness of sediments, and resonance frequency calculated by the H/V ratio of seismic noise for the Cologne area (Germany)," *Bulletin of the Seismological Society of America*, vol. 92, no. 6, pp. 2521–2527, 2002.

[5] J. K. Ahn, D. Y. Kwak, and H. S. Kim, "Estimating VS30 at Korean Peninsular seismic observatory stations using HVSR of event records," *Soil Dynamics and Earthquake Engineering*, vol. 146, Article ID 106650, 2021.

[6] R. D. Borcherdt, "Estimates of site-dependent response spectra for design (methodology and justification)," *Earthquake Spectra*, vol. 10, no. 4, pp. 617–653, 1994.

[7] S. R. Kotha, F. Cotton, and D. Bindi, "A new approach to site classification: mixed-effects Ground Motion Prediction Equation with spectral clustering of site amplification functions," *Soil Dynamics and Earthquake Engineering*, vol. 110, pp. 318–329, 2018.

[8] Gb 50011-2010, *Code for Seismic Design of Buildings*, Building Industry Press, Beijing, China, 2010.

[9] En 1998-1, *Eurocode 8: Design of concrete Structures-Part 1: General Rules, Seismic Actions and Rules for Buildings*, The European Union, Brussels, Belgium, 2004.

[10] O. Alonso-Pandavenes, G. Torres, F. J. Torrijo, and J. Garzón-Roca, "Basement tectonic structure and sediment thickness of a valley defined using HVSR geophysical investigation, Azuela valley, Ecuador," *Bulletin of Engineering Geology and the Environment*, vol. 81, no. 5, p. 210, 2022.

[11] C. J. Brown, *Mapping Bedrock Surface Contours Using the Horizontal-To-Vertical Spectral Ratio (HVSR) Method Near the Middle Quarter Area*, US Department of the Interior, US Geological Survey, Woodbury, Connecticut, 2013.

[12] M. Ibs-von Seht and J. Wohlenberg, "Microtremor measurements used to map thickness of soft sediments," *Bulletin of the Seismological Society of America*, vol. 89, no. 1, pp. 250–259, 1999.

[13] S. Maghami, A. Sohrabi-Bidar, S. Bignardi, A. Zarean, and M. Kamalian, "Extracting the shear wave velocity structure of deep alluviums of "Qom" Basin (Iran) employing HVSR inversion of microtremor recordings," *Journal of Applied Geophysics*, vol. 185, Article ID 104246, 2021.

[14] D. G. Mihaylov, *Seismic Microzonation of Great Toronto Area and Influence of Building Resonances on Measured Soil Responses*, The University of Western Ontario, Canada, 2011.

[15] S. P. Putti and N. Satyam, "Evaluation of site effects using HVSR microtremor measurements in Vishakhapatnam (India)," *Earth Systems and Environment*, vol. 4, no. 2, pp. 439–454, 2020.

[16] H. Seivane, A. García-Jerez, M. Navarro, L. Molina, and F. Navarro-Martínez, "On the use of the microtremor HVSR for tracking velocity changes: a case study in Campo de Dalías basin (SE Spain)," *Geophysical Journal International*, vol. 230, no. 1, pp. 542–564, 2022.

[17] A. P. Singh, A. Shukla, M. R. Kumar, and M. G. Thakkar, "Characterizing surface geology, liquefaction potential, and maximum intensity in the Kachchh seismic zone, Western India, through microtremor analysis," *Bulletin of the Seismological Society of America*, vol. 107, no. 3, pp. 1277–1292, 2017.

[18] J. Lermo and F. J. Chavez-Garcia, "Are microtremors useful in site response evaluation?" *Bulletin of the Seismological Society of America*, vol. 84, no. 5, pp. 1350–1364, 1994.

[19] Y. Nakamura, "A method for dynamic characteristics estimation of subsurface using microtremors on the ground surface," *Quarterly Reports of the Railway Technical Research Institute Tokyo*, vol. 30, pp. 25–33, 1989.

[20] B. R. Cox, T. Cheng, J. P. Vantassel, and L. Manuel, "A statistical representation and frequency-domain window-rejection algorithm for single-station HVSR measurements," *Geophysical Journal International*, vol. 221, no. 3, pp. 2170–2183, 2020.

[21] C. Zhu, M. Pilz, and F. Cotton, "Evaluation of a novel application of earthquake HVSR in site-specific amplification estimation," *Soil Dynamics and Earthquake Engineering*, vol. 139, Article ID 106301, 2020.

[22] C. Cornou, E. Chaljub, and S. Tsuno, "Real and synthetic ambient noise recordings in the Grenoble basin: reliability of the 3D numerical model," in *Proceeedings of the 14th World Conference on Earthquake Engineering*, Beijing, China, October 2008.

[23] D. Raptakis and K. Makra, "Shear wave velocity structure in western Thessaloniki (Greece) using mainly alternative SPAC method," *Soil Dynamics and Earthquake Engineering*, vol. 30, no. 4, pp. 202–214, 2010.

[24] O. Akin and N. Sayil, "Site characterization using surface wave methods in the ArsinTrabzon province, NE Turkey," *Environmental Earth Sciences*, vol. 75, pp. 72–17, 2016.

[25] J. Delgado, C. Lopez Casado, J. Giner, A. Estevez, A. Cuenca, and S. Molina, "Microtremors as a geophysical exploration tool: applications and limitations," *Pure and Applied Geophysics*, vol. 157, no. 9, pp. 1445–1462, 2000.

[26] J. S. Lin and Y. Y. Wang, "Observation and analysis of the earth microtremor of Quanzhou city," *China Earthguake Engineering Journal*, vol. 3, pp. 76–80, 1993.

[27] M. R. Gallipoli and M. Mucciarelli, "Comparison of site classification from VS30, VS10, and HVSR in Italy," *Bulletin of the Seismological Society of America*, vol. 99, no. 1, pp. 340–351, 2009.

[28] J. X. Zhao, K. Irikura, J. Zhang, and Y. Fukushima, "An empirical site-classification method for strong-motion stations in Japan using H/V response spectral ratio," *Bulletin of the Seismological Society of America*, vol. 96, no. 3, pp. 914–925, 2006.

[29] B. Hassani and G. M. Atkinson, "Site-effects model for central and Eastern North America based on peak frequency and

average shear-wave velocity," *Bulletin of the Seismological Society of America*, vol. 108, no. 1, pp. 338–350, 2018a.

[30] B. Hassani and G. M. Atkinson, "Application of a site-effects model based on peak frequency and average shear-wave velocity to California," *Bulletin of the Seismological Society of America*, vol. 108, no. 1, pp. 351–357, 2018b.

[31] S. Chen, J. Lei, and Y. Li, "Microtremor recording surveys to study the effects of seasonally frozen soil on site response," *Sensors*, vol. 23, no. 12, p. 5573, 2023.

[32] Koller and G. Martin, "Practical user guidelines and software for the implementation of the H/V ratio technique: measuring conditions, processing method and results interpretation," in *Proceedings of the 13th world conference in earthquake engineering*, Columbia, Canada, August 2004.

[33] P. Capizzi and R. Martorana, "Analysis of HVSR data using a modified centroid-based algorithm for near-surface geological reconstruction," *Geosciences*, vol. 12, no. 4, p. 147, 2022.

[34] A. P. Singh, B. Sairam, V. Pancholi, S. Chopra, and M. R. Kumar, "Delineation of thickness of intrabasaltic rocks beneath the Deccan volcanic province of western India through microtremor analysis," *Soil Dynamics and Earthquake Engineering*, vol. 138, Article ID 106348, 2020.

[35] W. H. Qi, "Comparison of fundamental periods of four type sites," *World Earthquake Engineering*, vol. 32, no. 3, pp. 48–52, 2016.

[36] S. Y. Chen, *Application Research of Cluster Analysis on Microtremor's H/V Spectra*, Institute of engineering mechanics, China earthquake administration (China), Harbin, China, 2019.

[37] Cecs, "Technical specification for surveying of site microseisms(TSSM)," vol. 74, p. 95, China Building Industry Press, Beijing, China, 1996.